Spring 2015

A novel entropy production based full-chip TSV fatigue analysis

Tianchen Wang

A NOVEL ENTROPY PRODUCTION BASED

FULL-CHIP TSV FATIGUE ANALYSIS

by

TIANCHEN WANG

A THESIS

Presented to the Faculty of the Graduate School of the

MISSOURI UNIVERSITY OF SCIENCE AND TECHNOLOGY

In Partial Fulfillment of the Requirements for the Degree

MASTER OF SCIENCE IN COMPUTER ENGINEERING

2015

Approved by

Dr. Yiyu Shi, Advisor
Dr. Sung Kyu Lim
Dr. Minsu Choi

ABSTRACT

Through-silicon vias (TSVs) are subject to thermal fatigue due to stress over time, no matter how small the stress is. Existing works on TSV fatigue all rely on measurement-based parameters to estimate the lifetime, and cannot consider detailed thermal profiles. In this paper, we propose a new method for TSV fatigue prediction using entropy production during thermal cycles. By combining thermodynamics and mechanics laws, the fatigue process can be quantitatively evaluated with detailed thermal profiles. Experimental results show that interestingly, the landing pad possesses the most easy-to-fail region, which generates up to 50% more entropy compared with the TSV body. The impact of landing pad dimension and TSV geometries are also studied, providing guidance for reliability enhancement. Finally, full-chip fatigue analysis is performed based on stress superposition. To the best of the authors' knowledge, this is the first TSV fatigue model that is free of measurement data fitting, the first that is capable of considering detailed thermal profiles, and the first framework for efficient full-chip TSV fatigue analysis.

ACKNOWLEDGMENTS

Foremost, I would like to express my sincere gratitude to my advisor Prof. Yiyu Shi for the continuous support of my master study and research, for his patience, motivation, enthusiasm, and immense knowledge. His guidance helped me in all the time of research and writing of this thesis. I could not have imagined having a better advisor and mentor for my study.

Besides my advisor, I would like to thank the rest of my thesis committee: Prof. Sung Kyu Lim and Prof Minsu Choi, for their encouragement, insightful comments, and hard questions.

My sincere thanks also goes to Prof. Sung Kyu Lim, for offering me the visiting student opportunities in his group and leading me working on diverse exciting project.

I thank my fellow labmates in Missouri S&T CAD Group: Hui Geng, Umamaheswara Rao Tida, Khalid K. Al-Jabery, Jinglan Liu, Qifeng Chen, Chunyu Wang, and Ying Zhang, for the stimulating discussions, for the sleepless nights we were working together before deadlines, and for all the fun we have had in the past. Also I thank my friends in Missouri S&T University: Wei Wang, Huixu Deng, Boyang Li and Fei Cheng. In particular, I am grateful to my girlfriend Shanshan Bi for enlightening me my life.

Last but not the least, I would like to thank my family: my parents Yi Wang and Yi Ma, for giving birth to me at the first place and supporting me spiritually throughout my life.

TABLE OF CONTENTS

Page

LIST OF ILLUSTRATIONS

Figure Page

LIST OF TABLES

1. INTRODUCTION

With the rapid growing requirements on the performance, speed and power of integrated circuits, tremendous efforts have been made towards the successful development of the three-dimensional integrated circuit (3D IC). Through-silicon vias (TSVs) play an important role in 3D ICs as vertical signal and power interconnects and facilitating heat transfer between different tiers.

Due to thermal loading, all electronic devices have limited lifetime restricted by thermal failures. In the application of 3D ICs, the mismatch of coefficients of thermal expansion (CTE) between copper, silicon dioxide and silicon leads to thermo-mechanical stress and strain at the interfaces. If the stress applied on a material is higher than its yield strength, it will start plastic deformation. Various literature have thus studied the algorithms to capture stress hotspots in a 3D IC(e.g.,[1, 2]). A less known and studied problem, on the other hand, is the thermal fatigue when the stress is below yield strength. With cyclic thermal loading, the stress and strain will cause elastic deformation, accumulating fatigue over time. Such fatigue will result in interfacial cracks between liner, substrate, landing pad and TSV body, as shown in Figure 1.1 [3]. It is essential to understand and investigate the mechanics of TSV fatigue and optimize chip designs for better performance, reliability and robustness.

The limited works available on TSV fatigue are mainly based on the Coffin-Manson model, the details of which will be discussed in Section 2.2. For example, Choa [4] studied the durability of TSV using the model by analyzing the plastic strain due to repetitive temperature cycling and investigated the impact of TSV design parameters. Ladani [5] applied the model in the reliability analysis of TSVs and solder joints as well as in the

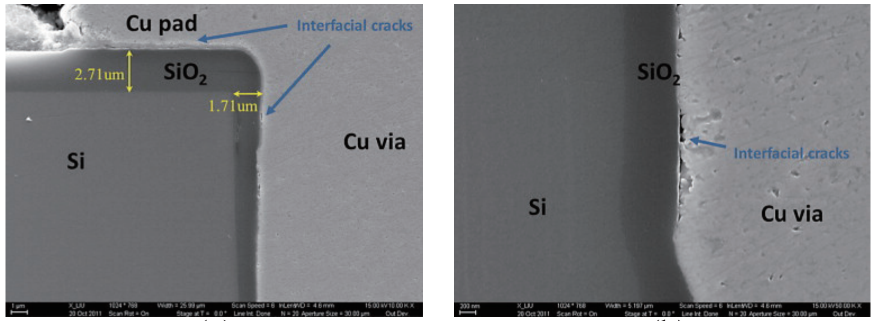

(a) (b)

Figure 1.1: SEM images of interfacial cracks under Cu pad and on the TSV side wall.

impact study of underfill thickness and stiffness. A few limitations exist for the Coffin-Mason model and thus all these methods. They require measurement data fitting, and cannot consider any thermal profile details during thermal cycling.

In this paper, we propose a novel model based on entropy production, which does not need any measurement data fitting, to quantitatively predict TSV fatigue during thermal cycles. The model takes detailed transient thermal profile into consideration. In addition, we show that the classic Coffin-Manson fatigue model can be deduced from our model, which partially verifies its correctness. We then further study the impact of TSV structures and locations on fatigue using our model. Finally, we present an efficient framework for full-chip fatigue analysis based on stress superposition. The main contribution of our paper is that we have proposed (1) the first TSV fatigue model that is free of measurement data fitting, and the first capable of considering detailed thermal profiles; (2) a few interesting observations on the impact of TSV structures and locations on fatigue; and (3) the first framework for full-chip TSV fatigue analysis.

The remainder of the paper is organized as follows: Section 2 reviews two models for mechanical reliability and thermal fatigue analysis, with their shortcomings. Section 3 theoretically introduces the novel entropy production fatigue analysis. Section 4 investigates the impact of TSV structures and locations, and Section 5 presents the full-chip TSV fatigue analysis framework. Concluding remarks are given in Section 6.

2. PRELIMINARIES

2.1. VON MISES STRESS CRITERION

When stress exceeds the yield strength, materials start to experience irreversible plastic deformation. The von Mises yield criterion is most widely used to determine whether an isotropic and ductile metal will yield when it is subject to a complex loading condition [6, 7].

The von Mises stress is derived from stress tensor, a combination of normal and shear stresses that has nine components and completely describes the state of a stress applied on an object at a point. The equation of stress tensor is shown in Eq. (2.1) and the related von Mises stress is shown in Eq. (2.2). The indices (*i*, *j*) in Eq. (2.2) refer to the normal and tangential directions of the stress, respectively. When *i* equals *j*, σ_{ij} is called normal stress and when *i* does not equal *j*, σ_{ij} is called shear stress.

$$\sigma = \sigma_{ij} = \begin{bmatrix} \sigma_{11} & \sigma_{12} & \sigma_{13} \\ \sigma_{21} & \sigma_{22} & \sigma_{23} \\ \sigma_{31} & \sigma_{32} & \sigma_{33} \end{bmatrix} \tag{2.1}$$

$$\sigma_v = [\frac{1}{2}(\sigma_{xx} - \sigma_{yy})^2 + \frac{1}{2}(\sigma_{yy} - \sigma_{zz})^2 + \frac{1}{2}(\sigma_{zz} - \sigma_{xx})^2 + 3(\sigma_{xy}^2 + \sigma_{yz}^2 + \sigma_{xz}^2)]^{\frac{1}{2}} \tag{2.2}$$

The von Mises criterion only shows whether a material starts plastic deformation during operation at a specific time, and therefore does not apply to long-term material fatigue analysis (especially when the stress does not exceed the yield strength).

2.2. EXISTING FATIGUE MODELS

Researchers have attempted to quantify material fatigue under various circumstances for many years. Miner [8] proposed the first idea about quantifying the fatigue damage under the assumption that the life fractions of individual amplitudes sum up to unity. From then on, various models for fatigue lifetime prediction were developed on different variables such as strain, stress, energy, damage, temperature, frequency, etc. Among them, the Coffin-Manson model is the most widely used one, which is based on plastic strain.

Depending on the strain amplitude ($\Delta\varepsilon$), the total number of cycles to failure (N_f) is depicted, with the fatigue ductility coefficient (ε'_f) and the fatigue ductility exponent (c) adopted for various materials by specific measurement data fitting. The equation is shown in Eq. (2.3).

$$\frac{\Delta\varepsilon}{2} = \varepsilon'_f(2N_f)^c \tag{2.3}$$

Since the Coffin-Manson model applies on the condition that the fatigue due to plastic deformation dominates, it is commonly combined with Basquin's equation to take elastic deformation into consideration, leading to Eq. (2.4).

$$\frac{\Delta\varepsilon}{2} = \frac{\sigma'_f}{E}(2N_f)^b + \varepsilon'_f(2N_f)^c \tag{2.4}$$

where σ'_f is the fatigue strength coefficient, E is the elastic modulus and b is the Basquin's exponent. This equation greatly improves the accuracy as it accounts the attribution of elastic deformation, especially in the higher reversals to failure area.

Two significant limitations exist for both models. First, they rely on measurement data, which are valid only under specific environmental conditions such as thermal shock and thermal cycles, to fit various parameters. As such, the fitted parameters are not suitable for all the complex conditions. Second, they only consider the effects of maximum temperature, temperature change, and cycling frequency, and are thus semi-empirical. For example, they cannot tell the difference between temperature cycle and thermal shock, where the ramp rate is the key difference. Thermal shock has much higher ramp rate, and results in more damage [9].

In this paper, we will propose a new model for TSV fatigue analysis that addresses both issues.

3. ENTROPY PRODUCTION MODELING

3.1. CONCEPT OF MODELING

The theory of fatigue prediction using entropy production is developed based on the Degradation-Entropy Generation (DEG) theorem. According to the second law of the thermodynamics, entropy is generated when the permanent degradation is presented through an irreversible process, which leads to a monotonic increase of disorder in a system. Therefore, the component of material degradation can be measured by entropy and thermodynamics energy [10, 11].

As for experimental validation, Naderi [12] validated the sufficient and necessary condition for the entropy production of a metal which takes cyclic loading before reaching the final fracture. In the experiment, it is observed that the metal specimen breaks during operation when its entropy production through thermal deformation cycles reaches a critical value. The behavior is independent of the loading type, the size and the geometry of the specimen. Furthermore, by applying the entropy degradation theory related thermodynamic forces, Amiri [13] experimentally determined the critical damage value of specimens subjected to different operations based on the entropy flow.

In this work, we take one step further and apply the concept of entropy generation to the context of TSV fatigue. Based on previous theories, when expressing the fact that the volumetric entropy production is positive, the Clausius-Duhem inequality (second law of thermodynamics) can be used

$$\dot{\gamma}(t) = \sigma(t) : \frac{\dot{\varepsilon}_p(t)}{T(t)} - J_q \frac{\text{grad}T(t)}{T^2(t)} \geq 0 \tag{3.1}$$

where J_q is the heat flux through the boundary, $\sigma(t)$is the symmetric stress tensor, $\dot{\gamma}(t)$is the entropy production, $\dot{\varepsilon_p}(t)$is the strain rate, $\sigma(t) : \dot{\varepsilon_p}(t) = \sigma_{ij}(t)\dot{\varepsilon}_{p(ij)}(t)$ is the tensor multiplication.

The heat flow and the work within an arbitrary control volume contribute to the total energy of a system, which describes the conservation of energy in thermodynamics. By introducing temperature and total strain, the coupling of thermodynamics and continuum mechanics can lead to an energy balance as shown in Eq. (3.2), made by heat conduction ($k\nabla^2 T(t)$), thermal inertia retardation effect ($\rho C\dot{T}$), internal heat generation through plastic deformation ($\sigma(t) : \dot{\varepsilon_p}(t)$) and thermo-elastic coupling ($T(t)\partial\sigma/\partial T(t) : \dot{\varepsilon_e}(t)$).

$$k\nabla^2 T(t) = \rho C\dot{T} - \sigma(t) : \dot{\varepsilon_p}(t) - \frac{T(t)\partial\sigma}{\partial T(t)} : \dot{\varepsilon_e}(t) \tag{3.2}$$

Then the entropy production during a certain period of time (γ_c) can be obtained by combining Eq. (3.1) and Eq. (3.2) with time integration, shown in Eq. (3.3).

$$\gamma_c = \int_0^t (\frac{W(t)}{T(t)} - \frac{J_q \cdot \text{grad}T(t)}{T^2(t)})\, dt \tag{3.3}$$

Subsequently, the material fatigue status of TSV is obtained based on entropy production. A larger entropy production means shorter lifetime due to fatigue. Apparently, the above model does not have any parameter that needs to be fitted, and considers the detailed thermal profile $T(t)$.

To conclude, comparisons between the von Mises stress, the Coffin-Manson model and our entropy production model are summarized in Table 3.1.

Table 3.1: Comparisons Between the Von Mises Stress, the Coffin-Manson Model and the Entropy Production Model.

	Von Mises stress	Coffin-Manson model	Entropy production
Fatigue life prediction		$\surd$	$\surd$
Consider detailed thermal profiles	$\surd$		$\surd$
No measurement data needed	$\surd$		$\surd$
Stress analysis	$\surd$		
Fatigue analysis		$\surd$	$\surd$

3.2. RELATIONSHIP TO COFFIN-MANSON MODEL

To partially validate our entropy production model, we will show in this section that the widely used Coffin-Manson model (i.e., Eq. (2.3)) can be deduced from Eq. (3.3) by making reasonable assumptions.

As the Coffin-Manson model applies the condition that plastic deformation dominates the fatigue of a material, we only consider the entropy production due to plastic deformation. First we introduce the model from Morrow [14], in which the plastic strain energy per cycle keeps approximately constant during the fully reversed experimental fatigue tests. The related equation is

$$\Delta w_p = \frac{4\sigma'_f(\frac{1-n'}{1+n'})}{\varepsilon'_f}(\frac{\Delta\varepsilon_p}{2})^{1+n'} \tag{3.4}$$

Assuming that we are dealing with low-cycle fatigue in small volume with heat conduction neglected, Eq. (3.4) leads to

$$\gamma_f = \int_0^t (\frac{f(t)\Delta w_p}{T(t)})\,dt \tag{3.5}$$

where $f(t)$ is the fraction of work done by plastic deformation during thermal cycles.

Then, by assuming the plastic energy dissipation and the temperature are constants throughout the thermal cycles, Eq. (3.5) leads to

$$\gamma_f = \frac{\Delta w_p}{T} N_f \tag{3.6}$$

Therefore, the number of cycles to failure N_f is obtained by employing Eq. (3.4), which is

$$N_f = \frac{T\gamma_f(\varepsilon'_f)^{n'}}{4\sigma'_f(\frac{1-n'}{1+n'})}(\frac{\Delta\varepsilon_p}{2})^{-(1+n')} \tag{3.7}$$

Compared with Coffin Mason model, we get

$$c = -\frac{1}{1+n'}, \varepsilon'_f = (\frac{2\sigma'_f(\frac{1-n'}{1+n'})}{T\gamma_f(\varepsilon'_f)^{n'}})^{-\frac{1}{1+n'}} \tag{3.8}$$

This leads to the conclusion that Coffin-Manson model is a special case of our entropy generation model under specific assumptions and simplifications, which partially validates the correctness of our model. In the future, we will validate our model directly with measurement data.

3.3. EXPERIMENTAL VALIDATION OF ENTROPY PRODUCTION

In the previous section, we have demonstrate that our entropy production method is more generalized than Coffin-Manson model. To validate it experimentally, we use the via chain test structures, which would form part of 3D ICs [15] with measurement data for silicon correlation.

As shown in Figure 3.1(a), the stacked via chain structure is used for reliability evaluation. It is made of two SiLK levels and two SiO_2 levels upper placed, with three metal levels (MC, M1 and M2) connected by two level of vias (V1 and V2). In the experiment, the chain has 50 links repeatedly, alternating between M2 and MC, which are local interconnects linking to other stacks. Therefore, this unsymmetrical structure would lead to a non-homogeneous stress on vias.

In Figure 3.1(b), the SEM cross section view clearly shows the typical fail at the stress condition of certain thermal cycles, occurred along the (111) plane.

To model the via structure, the geometry of the structures applied in the experimental test were adopted from [16]. The entropy production result of via with cross-section view is shown in Figure 3.1(c). The highest entropy production occurs on upper-right and bottom-left parts, leading to the crack shears through the entire via. The nonsymmetrical crack is due to the stacked via test structure: Repeated units of metal levels in the test structure are connected by two levels of vias, with a nonsymmetrical configuration. This result agrees well with the crack plane in Figure 3.1(b), showing a precise fatigue prediction of entropy production method.

To compare entropy production with Coffin-Manson prediction, four different thermal profiles are used. The parameters of Coffin-Manson equation vary due to various experimental environments [4, 17, 18] and yield multiple results. The resulting cycles to failure from measurement, entropy production and Coffin-Manson equation are shown in Figure 3.1(d). ΔT means the temperature difference in thermal cycles, while cycles to failure in y axis is in log scale. Noted that the measurement data uses N_{50} median number, and the entropy production prediction is determined by the result of 215°C.

As shown in the figure, the curves of Coffin-Manson exhibits a large range of uncertainties in y-axis (cycles to failure). In practical application, it is hard to decide which parameters should be used, which depends on specific working environment. By setting total entropy production value, the curve fits well with experiment data along higher temperature difference area. Entropy production has a better fatigue prediction performance than Coffin-Manson in practical application.

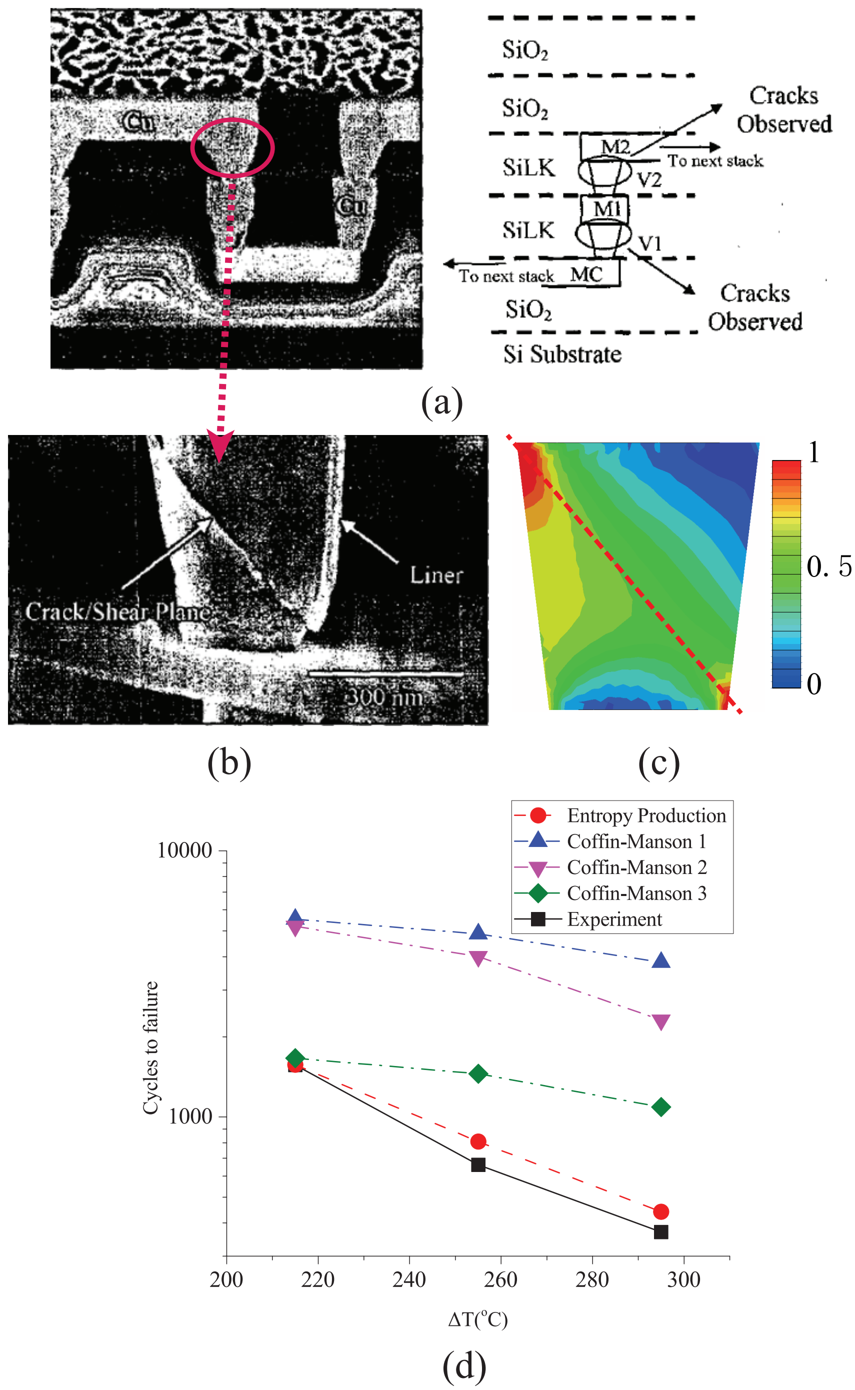

Figure 3.1: SEM image showing shearing and cracking in via after thermal cycles, cross-sectional view of via in entropy production modeling and cycles to failure of experiment test, entropy production and Coffin-Manson prediction.

4. SIMULATION AND ANALYSIS

4.1. IMPACT OF THERMAL CYCLES

In this section, TSV cells are modeled in Abaqus to calculate the entropy production of TSV for fatigue prediction. For the first part of the simulation, a single TSV cell with a copper TSV body and two landing pads attached is built as shown in Figure 4.1(a)(b).

Unless specified, the geometries are the same as in [7]. The parameters of materials applied are listed in Table 4.1. In this model, we have simplified the bottom part of the TSV by ignoring the solder joint attached. The top part is modeled accurately for fatigue analysis. The interfaces between different parts are assumed to be perfectly adhesive. The thermal cycles range from 20°C to 70°C, as shown in Figure 4.1(c). Note that this temperature profile is derived from actual operating conditions of a chip.

It needs to be clarified that since entropy production has only been experimentally proved on metals, our fatigue analysis only focuses on the TSV body and the attached landing pad. In other words, it is limited to copper. In addition, in all the figures afterwards, we use a single color bar for all the parts in the same figure for better comparison.

We simulate the TSV structure for five thermal cycles. The resulting entropy production distributions on the top and bottom surfaces of the landing pad attached to the top surface of the TSV are shown in Figure 4.2.

It is clear that after five thermal cycles, the entropy production at the four corners of the landing pad increases much faster than that at the center. The reason is that the expansion and contraction of the TSV body has little axial effect on the attached area between the TSV body and the landing pad, since they have the same CTE. However, the corners of the landing pad located between the dielectric layer and ILD have larger moments during deformation, thus leading to higher entropy production.

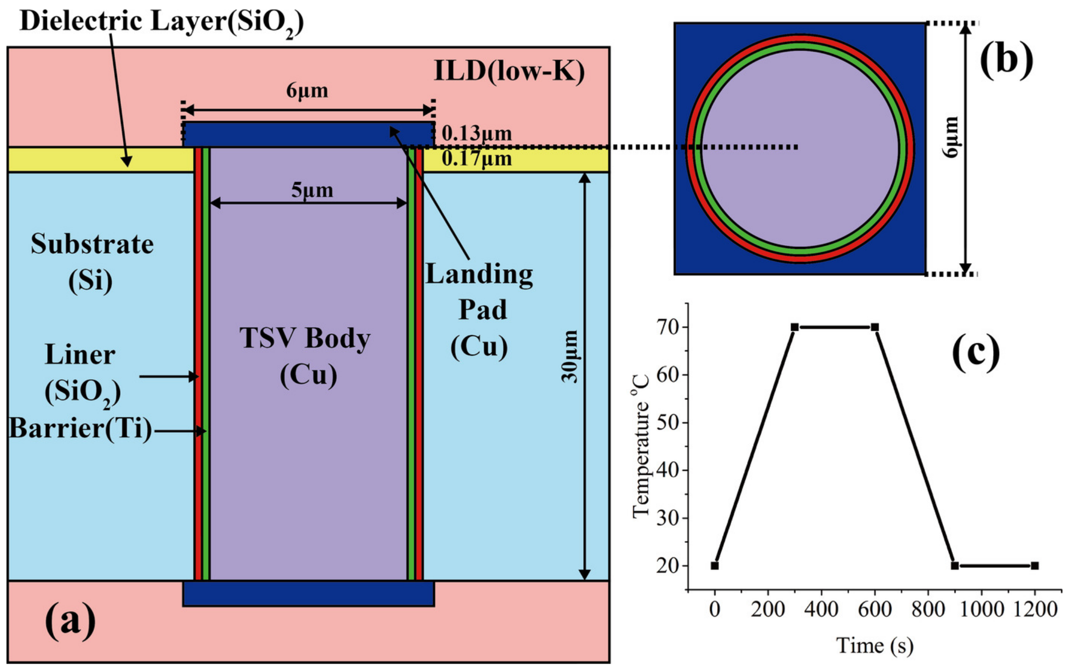

Figure 4.1: Illustration of the side view and the top view of the TSV structure, with the profile of a thermal cycle.

The results of the TSV body are shown in Figure 4.3, with its inner surface, outer surface and top surface displayed. After the thermal cycles, the outer edge of the top surface has the maximum entropy production. This is again due to the CTE mismatch between the TSV body and the barrier, which causes large stress and strain on the top interface. In addition, the minimum entropy production area can be found in the middle part of the top surface, as it is attached to the landing pad with the same CTE. Finally, due to the radial

Table 4.1: Material Properties

Material	CTE (ppm/K)	Young's Modulus(GPa)	Poisson's ratio
Cu	17	110	0.35
Si	2.3	130	0.28
SiO_2	0.5	71	0.16
Low K	20	9.5	0.3
BCB	40	3	0.34
Ti	8.6	116	0.32

effect of stress, the entropy production also concentrates in the middle of the TSV body, which increases at about 50% higher rate than the neighboring parts. This suggests that the middle part of a TSV body can be a new reliability concern in the presence of fatigue.

In the simulations, we also discover that the rate of entropy production increase in the landing pad and the TSV body through cycles remain the same. Thus, single cycle modeling is sufficient for TSV fatigue analysis using entropy production, which will be used in the remaining of the paper.

We summarize the important findings from the above study as follows.

Observation 1: Landing pads have maximum entropy production located at corners.

Observation 2: The middle part of a TSV body shows concentrated entropy production, leading to a new reliability concern.

As illustrated in previous section, the Coffin-Manson method only considers the maximum strain amplitude during the thermal cycles. Therefore, to prove the capable of considering detailed thermal profiles of entropy production, the TSV models with four different thermal cycles are built for comparison, shown in Figure. 4.4. The four thermal cycles have the same cycle time and temperature range, leading to the same Coffin-Manson

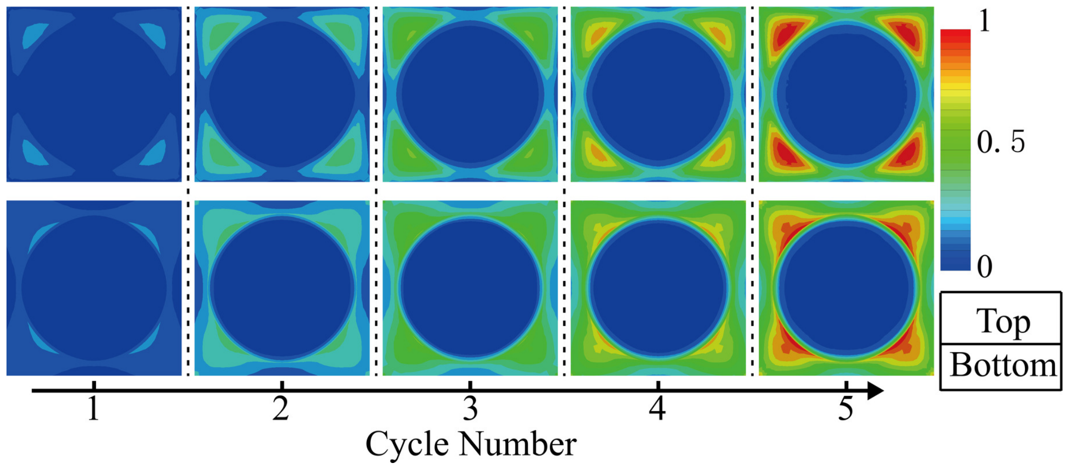

Figure 4.2: Entropy production distributions on the top and bottom surfaces of the landing pad through five thermal cycles.

fatigue prediction. The four cycles have different rate of temperature change and distribution. Group 1 and 2, 3 and 4 have the same high temperature period, while group 1 and 3 , 2 and 4 has the same rates of temperature change. The results are shown in Table. 4.2.

The results clearly illustrate that the time period of high temperature doesn't influence the fatigue within entropy production, while the rate of temperature change does influence. It is observed that the results of group 2 and 4 with a higher temperature change rate have higher entropy production, in both landing pad and TSV body. This is caused by the nonlinear increasing of entropy production in plastic deformation at high stress. The higher temperature change rate, the higher entropy production leading to easier fatigue of material. Therefore, the entropy production fatigue method is applicable in the fatigue analysis considering the impact of different thermal cycles.

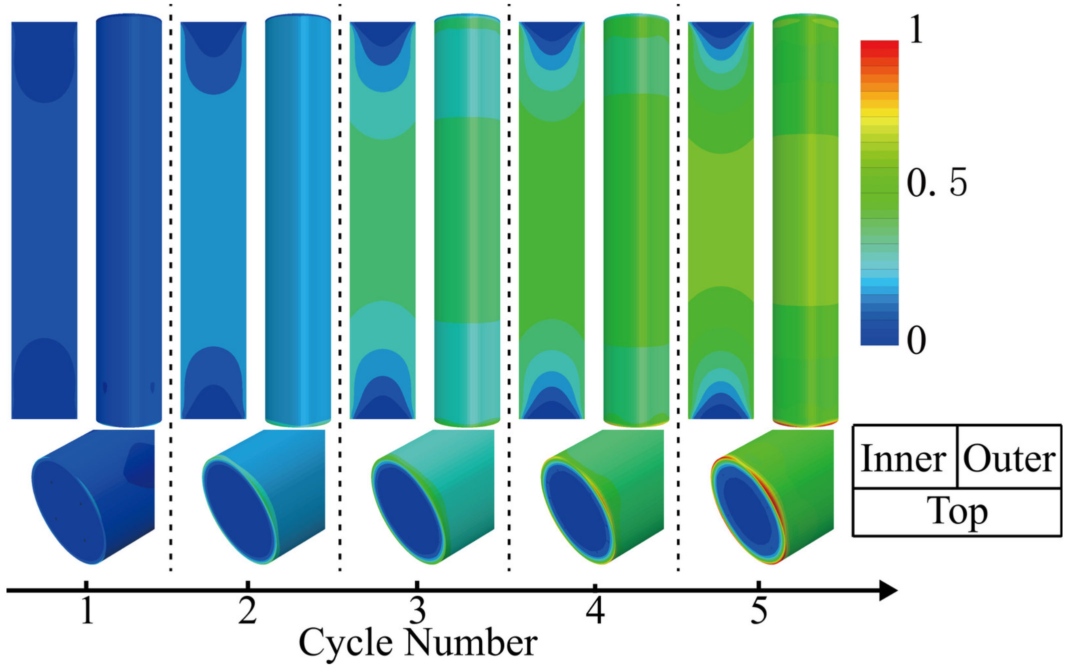

Figure 4.3: Entropy production distributions on the inner surface, outer surface and top surface of the TSV body through five thermal cycles.

4.2. IMPACT OF TSV STRUCTURE PARAMETERS

In this section, we study the impact of TSV structure parameters on the entropy production in a single TSV cell, hoping to establish guidelines for reliability optimization. We only focus on the maximum entropy production values of the TSV body and the landing pad respectively, which provide information about the most dangerous areas.

The results of entropy production of the landing pad and the TSV body with different thickness and width of the landing pad, thickness of the liner and length of the TSV body are shown in Figure 4.5.

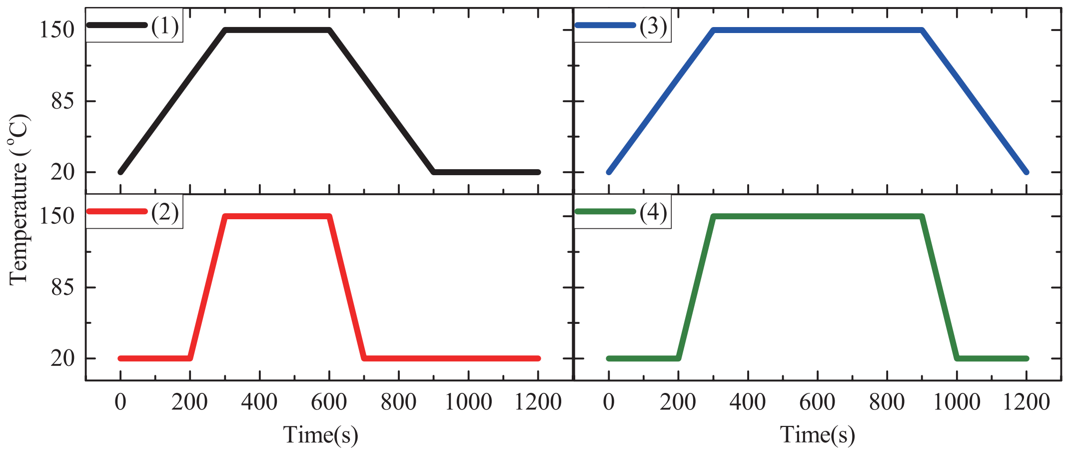

Figure 4.4: Thermal profiles for entropy production validation.

First of all, from Figure 4.5 we can first see that in all the cases, the landing pad always has a much higher maximum entropy production compared with the TSV body. For example, when the landing pad thickness is 0.1 μm, the maximum entropy production of the landing pad is approximately 50% higher than that of the TSV body.

Observation 3: More attention should be paid to the landing pad than the TSV body in terms of thermal fatigue during TSV cell designs.

In addition, from Figure 4.5(a) we can see that when the thickness of the landing pad increases, the maximum entropy production value of the landing pad decreases while that of the TSV body increases. This is because with the increase of thickness the landing pad gets stronger to hold against the deformation from the TSV body along the axial direction. As such, the strain rate gets smaller and the entropy production becomes smaller. As for the TSV body, a stronger landing pad leads to more stress on the surface, resulting in higher entropy production.

Table 4.2: Entropy production of TSV body and landing pad with different thermal cycles.

Thermal Profile Groups		1	2	3	4
Landing Pad	Max Entropy Production($\times 10^8 \mathrm{J/m^3K}$)	45.4	46.6	45.4	46.6
TSV Body		28.0	28.9	28.0	28.9

Observation 4: Increasing the thickness of the landing pad is helpful for the landing pad to reduce fatigue, but harmful for the TSV body.

Moreover, from Figure 4.5(b) we can see that as the width of the landing pad increases from 6 µm to 9 µm, the maximum entropy production values of both the landing pad and the TSV body increase. For the landing pad, this is because a wider landing pad introduces larger strain rate due to longer distance. For the TSV body, the stress acted on it remains the same while the strain rate increases. Therefore, increasing the width of the landing pad is not preferred for fatigue reduction.

Observation 5: Increasing the width of the landing pad is harmful for both the landing pad and the TSV body.

Furthermore, from Figure 4.5(c) we can see that as the thickness of the liner increases, the maximum entropy production value of the landing pad increases while that of the TSV body decreases, with very small differences. This is because the liner is made of silicon dioxide, which has a much lower CTE than copper. When the liner thickness increases, a more rigid wall is built around the TSV body, which holds against the landing pad. This causes the landing pad harder to deform, thus an increased stress on the interface between the liner and the landing pad. For the TSV body, the outer edge of the top surface has less strain rate than before, which leads to a slightly decreased maximum entropy production value.

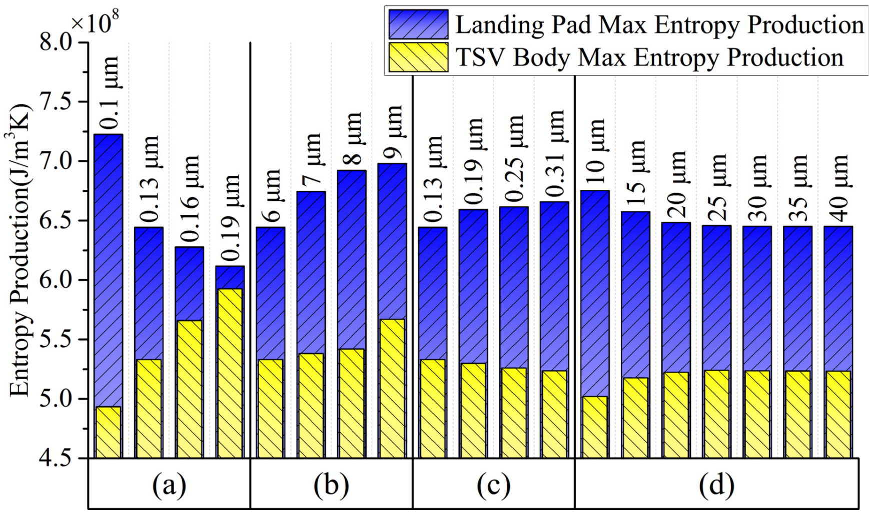

Figure 4.5: The maximum entropy production values of the landing pad and the TSV body, with various thickness and width of the landing pad, thickness of the liner and length of the TSV body, respectively.

Observation 6: The thickness of the liner has limited impact on the fatigue of both the landing pad and the TSV body.

Finally, from Figure 4.5(d) we can see that when the length of the TSV body is below 20 μm or aspect ratio 4:1, the maximum entropy production value of the landing pad decreases and that of the TSV body increases with the increase of the TSV body length. Both stop changing afterwards. This is because when the TSV body is long enough, the stress from expansion and contraction along the axial direction at the top surface does not change any more.

Observation 7: Aspect ratio of the TSV body only matters when it is small. In such scenarios, increasing the aspect ratio is helpful for the landing pad to reduce fatigue, but harmful for the TSV body.

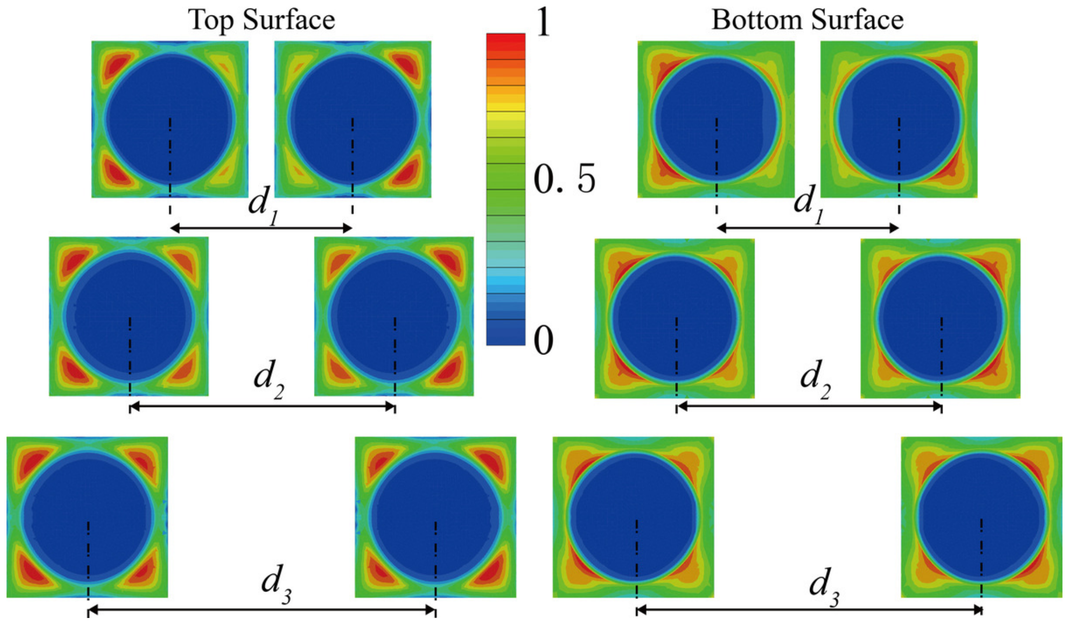

Figure 4.6: The entropy production distribution on the top and bottom surfaces of the landing pads in a TSV pair.

In this section, we study the impact of the pitch in a TSV pair. The entropy production distributions on the landing pads with different pitches (d_1 = 7 µm, d_2 = 10 µm, d_3 = 13 µm) are shown in Figure 4.6. From the figure, it is clear that the pitch affects the entropy production on both surfaces of the landing pad. When the TSVs get closer, the two inner corners on each landing pad have lower entropy production. This difference is caused by the silicon between the two TSVs. Small volume has less restricted power and since copper has a much higher CTE, the stress applied on the inner sides would decrease. Meanwhile on the contrary, the outer sides of both landing pads would be subject to more stress from the TSV body, leading to a higher entropy production.

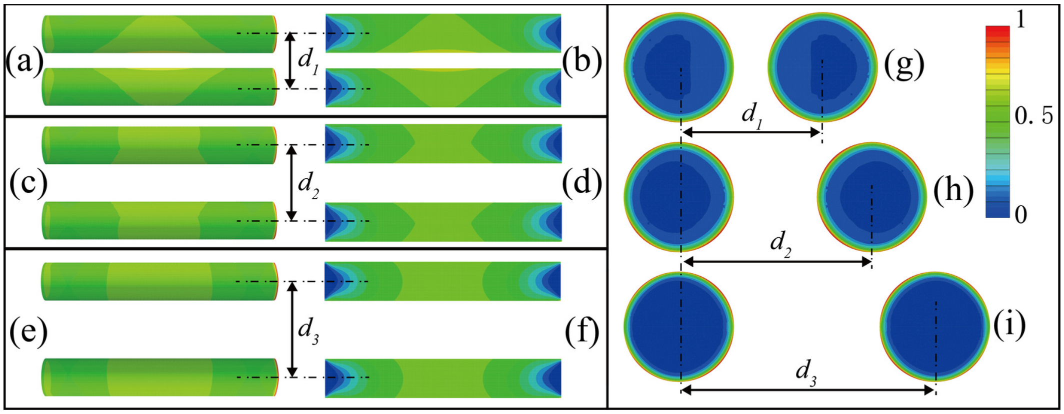

Figure 4.7: The entropy production distribution on the outer surface, inner surface and top surface of the TSV body in a TSV pair.

The corresponding entropy production distributions on the inner surface (b,d,f), outer surface (a, c, e) and top surface (g, h, i) of the TSV body are shown in Figure 4.7. From the figure we can tell that when the TSVs get closer, there is an easy-to-fail area in the middle part of the TSV body. Unlike the landing pad, the area closer to the other TSV body shows a higher entropy production. However, when the pitch increases, the distribution of entropy production becomes uniform, which is similar as the result of the single TSV model. The top surface of the TSV also shows the trend that the smaller pitch, the larger entropy production.

4.3. IMPACT OF THE PITCH IN A TSV PAIR

In this section, we study the impact of the pitch in a TSV pair. The entropy production distributions on the landing pads with different pitches are shown in Figure 4.6. From the figure, it is clear that the pitch affects the entropy production on both surfaces of the landing pad. When the TSVs get closer, the two inner corners on each landing pad have lower entropy production. This difference is caused by the silicon between the two TSVs. Small volume has less restricted power and since copper has a much higher CTE, the stress applied on the inner sides would decrease. Meanwhile on the contrary, the outer sides of both landing pads would be subject to more stress from the TSV body, leading to a higher entropy production.

The corresponding entropy production distributions on the inner surface, outer surface and top surface of the TSV body are shown in Figure 4.7. From the figure we can tell that when the TSVs get closer, there is an easy-to-fail area in the middle part of the TSV body. Unlike the landing pad, the area closer to the other TSV body shows a higher entropy production. However, when the pitch increases, the distribution of entropy production becomes uniform, which is similar as the result of the single TSV model. The top surface of the TSV also shows the trend that the smaller pitch, the larger entropy production.

Finally, Figure 4.8 with various pitches (d_1 = 7 µm, d_2 = 10 µm, d_3 = 13 µm) presents the maximum entropy production value of both the landing pad and the TSV body for various pitches. From the figure we can see that with the increase of the pitch, the maximum entropy production value of both the landing pad and the TSV body reduces.

Observation 8: Increasing the TSV pitch is helpful for both the landing pad and the TSV body to reduce fatigue.

4.4. IMPACT OF LANDING PAD ORIENTATION IN ARRAYS

The entropy production distribution depends on the configuration of TSV array. The TSV fatigue with various TSV array while retaining the same TSV density have been studied by [19]. However, the impact of TSV array configuration on landing pad has not been investigated before. As the previous section shows, the landing pad always has a higher entropy production compared with TSV body during thermal cycles, that attract

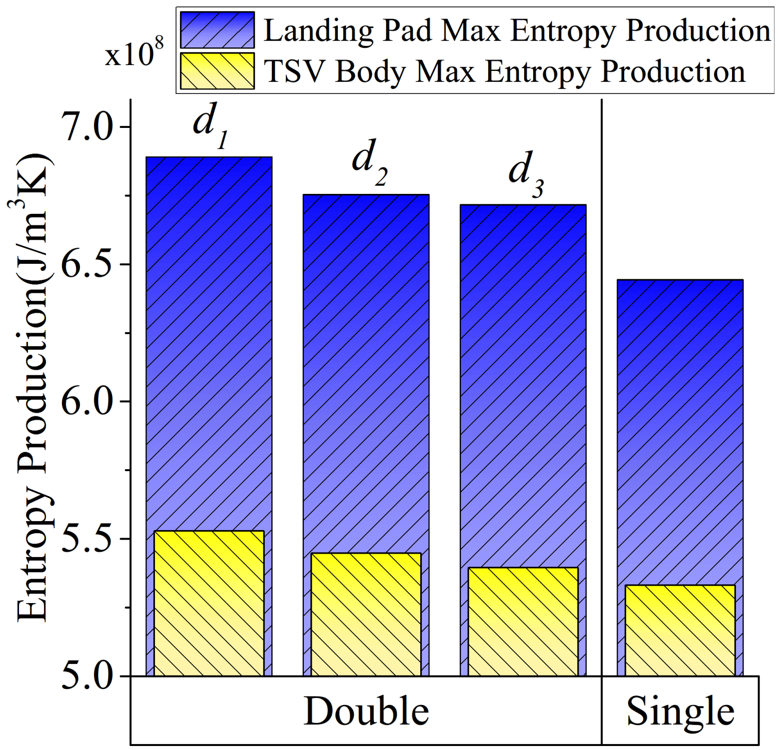

Figure 4.8: The maximum entropy production of the landing pad and the TSV body, with various pitches.

more attention on fatigue preventing. Therefore, two arrays with different landing pad orientations and same TSV density are modeled for comparison, shown in Figure. 4.9(a) and (b). The angles of the landing pad in two groups have a difference of 45 degree. Models with various pitch sizes are built for comparison.

The results are shown in Figure. 4.9(c) with five different pitch size groups. It is observed that the maximum entropy production of landing pad is higher than that of TSV body as the same as before. The larger pitch size causes the lower entropy production, for both TSV body and landing pad. For most cases, the entropy productions of TSV body and landing pad in group (b) is lower than those in group (a). The only exception is the TSV body entropy production with pitch size is $10\,\mu m$, where the distance between two landing pads is as small as $1.5\,\mu m$. This is caused by close interact of each landing pads, which occur a high stress effect on the other TSV body. Therefore, the fatigue tradeoff between landing pad and TSV bdoy needs to be made when TSV pitch is small enough. In most cases, the TSV layout with landing pad orientation as Figure. 4.9(b) is preferred.

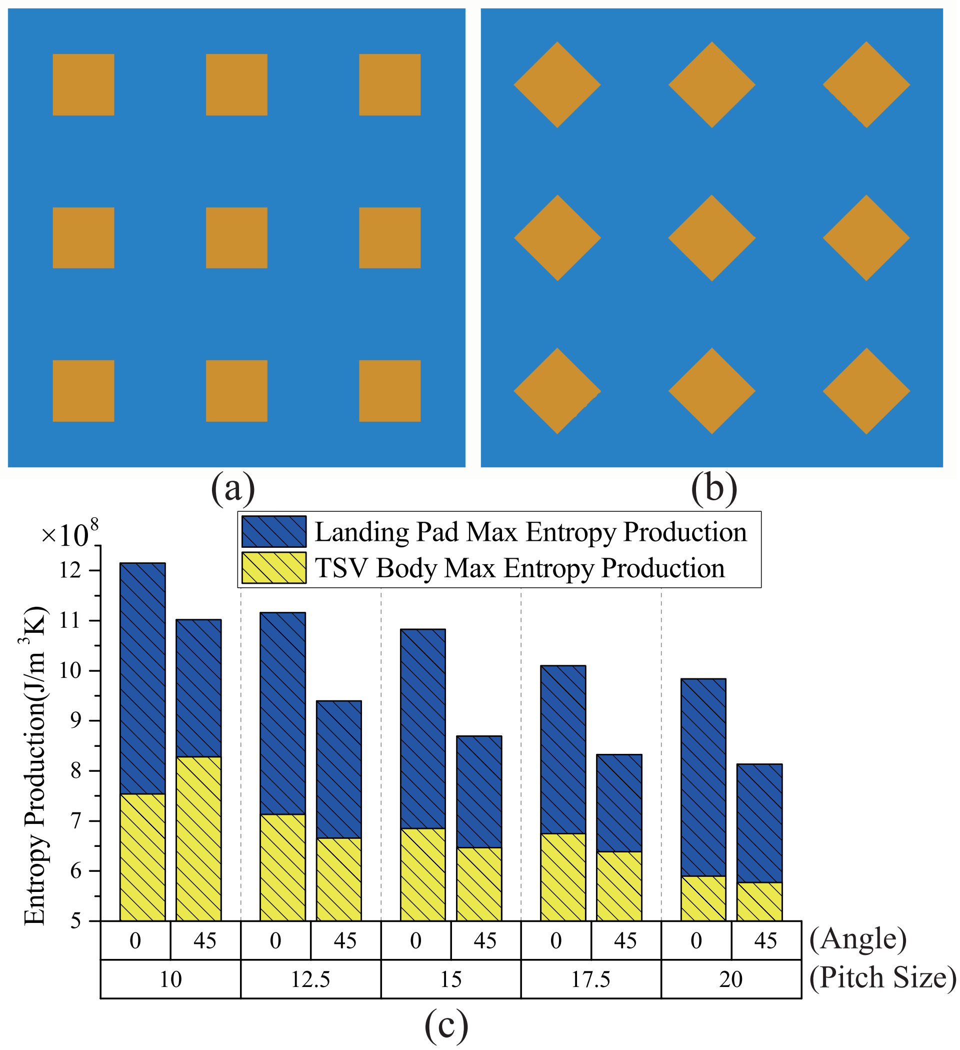

Figure 4.9: The two layouts of TSV arrays and the corresponding results.

5. FULL CHIP ANALYSIS

FEA analysis of TSV fatigue using entropy production for a single TSV and a TSV pair has been investigated in the previous section. However, FEA is limited to small scale simulation due to the computational complexity. Therefore, it is necessary to develop a fast and accurate framework to analyze the fatigue of TSVs at full-chip scale. Superposition is the best approach in this context, but unfortunately, the entropy production as can be seen from Eq. (3.3) is nonlinear and cannot be superposed. Accordingly, we propose to use stress tensor superposition to achieve this target. The validity of stress tensor superposition has been verified in [7]. With the full-chip stress obtained from superposition, the strain can be obtained by fitting Hooke's law and the strain-stress curve of copper. The entropy production can then be readily derived.

To validate the correctness of our framework, the layout of a TSV pair is simulated by both FEA and our framework, with results shown in Figure 5.1. Note that the landing pads are not included in the analysis. It can be clearly seen that the patterns from both exactly match. The meshes in Figure 5.1(b) is the computation grid used to perform the superposition of stress.

Now we are ready to apply our framework to full-chip analysis. We apply two TSV placement styles on the same design with the same TSV cell size. A total of 1,472 TSVs are placed in a chip area of 1 mm $\times$ 1 mm. In the regular placement the TSVs are uniformly placed with 25 μm pitch as shown in Figure 5.2(a). The irregular placement, as shown in Figure 5.2(b), results in shorter wirelength. The minimum TSV pitch is 10 μm. Comparing the two maps, the irregular TSV placement results in 17.3$\times$ higher maximum entropy production during thermal cycles. In addition, in the irregular placement, the hot-pots are mainly located at places where the TSVs have small pitches. Meanwhile in the regular placement with much larger pitches, almost identical entropy production occurs at

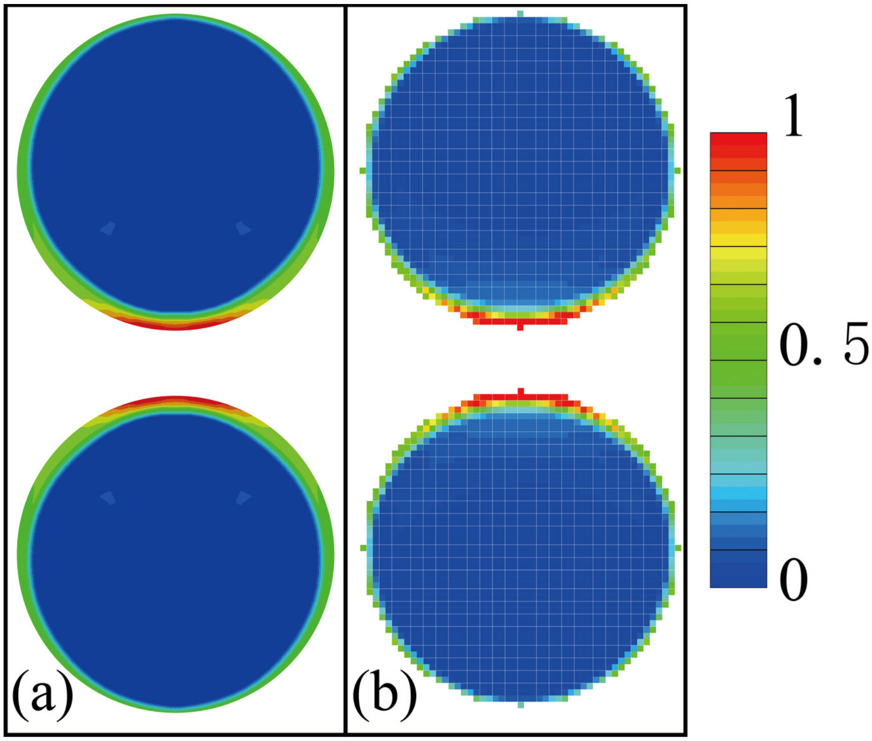

Figure 5.1: Entropy production distributions on the top surfaces of a TSV pair using FEA and our framework.

each TSV. Therefore, we can conclude that full-chip TSV placement needs to consider the tradeoff between wirelength and TSV fatigue.

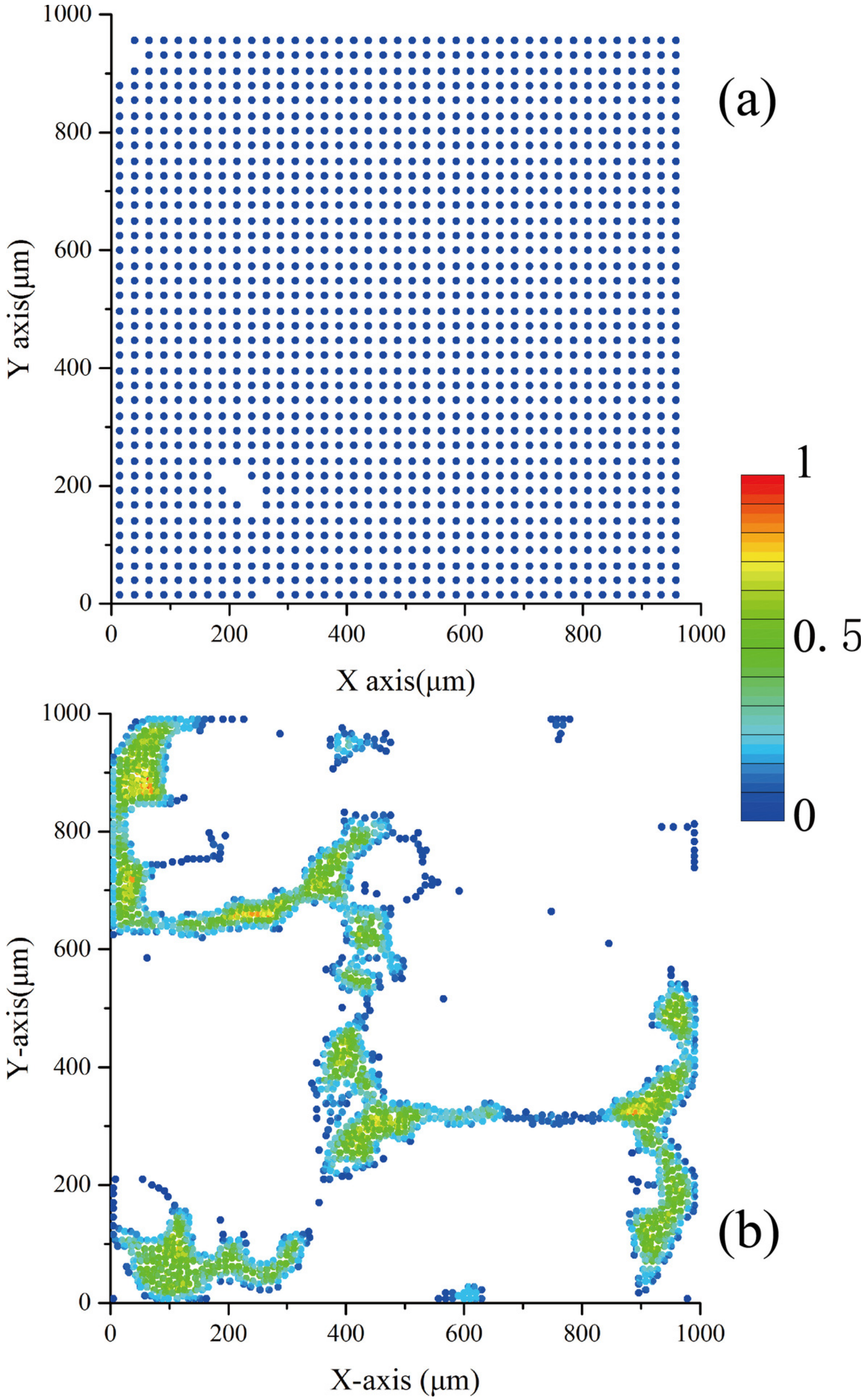

Figure 5.2: Entropy production distributions of full-chip TSVs in regular and irregular layouts.

6. CONCLUSIONS

In this paper, a new TSV fatigue model based on entropy production has been proposed. By combining thermodynamics and mechanics laws, the fatigue process can be quantitatively evaluated with the model. Experimental results show many interesting and important observations on the impact of TSV structure and location, providing guidance for reliability enhancement. Finally, full-chip fatigue analysis is performed based on stress superposition. To the best of the authors' knowledge, this is the first TSV fatigue model that is free of measurement data fitting, the first that is capable of considering detailed thermal profiles, and the first framework for efficient full-chip TSV fatigue analysis.

BIBLIOGRAPHY

[1] Moongon Jung, David Z Pan, and Sung Kyu Lim. Chip/package co-analysis of thermo-mechanical stress and reliability in tsv-based 3d ics. In *Proceedings of the 49th Annual Design Automation Conference*, pages 317–326. ACM, 2012.

[2] Kuan H Lu, Suk-Kyu Ryu, Qiu Zhao, Xuefeng Zhang, Jay Im, Rui Huang, and Paul S Ho. Thermal stress induced delamination of through silicon vias in 3-d interconnects. In *Electronic Components and Technology Conference (ECTC), 2010 Proceedings 60th*, pages 40–45. IEEE, 2010.

[3] Xi Liu, Qiao Chen, Venkatesh Sundaram, Rao R Tummala, and Suresh K Sitaraman. Failure analysis of through-silicon vias in free-standing wafer under thermal-shock test. *Microelectronics Reliability*, 53(1):70–78, 2013.

[4] Sung-Hoon Choa, Cha Gyu Song, and Haeng Soo Lee. Investigation of durability of tsv interconnect by numerical thermal fatigue analysis. *International Journal of Precision Engineering and Manufacturing*, 12(4):589–596, 2011.

[5] Leila J Ladani. Numerical analysis of thermo-mechanical reliability of through silicon vias (tsvs) and solder interconnects in 3-dimensional integrated circuits. *Microelectronic Engineering*, 87(2):208–215, 2010.

[6] Joseph Edward Shigley. *Mechanical engineering design*. McGraw-Hill, 1972.

[7] Moongon Jung, Joydeep Mitra, David Z Pan, and Sung Kyu Lim. Tsv stress-aware full-chip mechanical reliability analysis and optimization for 3d ic. *Communications of the ACM*, 57(1):107–115, 2014.

[8] Milton A Miner et al. Cumulative damage in fatigue. *Journal of applied mechanics*, 12(3):159–164, 1945.

[9] Rakesh K Agarwal, L Tuchscherer, H Cui, R Jain, T Torri, and S Baxter. Thermal cycling and thermal shock for fcob testing. *ASME EEP*, 26:2, 1999.

[10] C Basaran and C-Y Yan. A thermodynamic framework for damage mechanics of solder joints. *Journal of Electronic Packaging*, 120(4):379–384, 1998.

[11] MD Bryant, MM Khonsari, and FF Ling. On the thermodynamics of degradation. *Proceedings of the Royal Society A: Mathematical, Physical and Engineering Science*, 464(2096):2001–2014, 2008.

[12] M Naderi, M Amiri, and MM Khonsari. On the thermodynamic entropy of fatigue fracture. *Proceedings of the Royal Society A: Mathematical, Physical and Engineering Science*, page rspa20090348, 2009.

[13] M Amiri, M Naderi, and MICHAEL M Khonsari. An experimental approach to evaluate the critical damage. *International Journal of Damage Mechanics*, 20(1):89–112, 2011.

[14] JoDean Morrow. Cyclic plastic strain energy and fatigue of metals. *Internal Friction, Damping and Cyclic Plasticitiy, STP378*, pages 45–84, July 1965.

[15] RG Filippi, JF McGrath, TM Shaw, CE Murray, HS Rathore, PS McLaughlin, V McGahay, L Nicholson, P-C Wang, JR Lloyd, et al. Thermal cycle reliability of stacked via structures with copper metallization and an organic low-k dielectric. In *Reliability Physics Symposium Proceedings, 2004. 42nd Annual. 2004 IEEE International*, pages 61–67. IEEE, 2004.

[16] Jing Zhang, Max O Bloomfield, Jian-Qiang Lu, Ronald J Gutmann, and Timothy S Cale. Modeling thermal stresses in 3-d ic interwafer interconnects. *Semiconductor Manufacturing, IEEE Transactions on*, 19(4):437–448, 2006.

[17] Qiao Chen, Xi Liu, Venkatesh Sundaram, S Sitaraman, and R Tummala. Double-side process and reliability of through-silicon vias (tsvs) for passive interposer applications. 2014.

[18] TH Low and John HL Pang. Modeling plated copper interconnections in a bumpless flip chip package. In *Electronics Packaging Technology, 2003 5th Conference (EPTC 2003)*, pages 791–796. IEEE, 2003.

[19] Kuan H Lu, Xuefeng Zhang, Suk-Kyu Ryu, Jay Im, Rui Huang, and Paul S Ho. Thermo-mechanical reliability of 3-d ics containing through silicon vias. In *Electronic Components and Technology Conference, 2009. ECTC 2009. 59th*, pages 630–634. IEEE, 2009.

VITA

Tianchen Wang was born in China in 1987. He earned a bachelor's degree of science and a master's degree of science in mechanical engineering, both at North China Electric Power University, 2010 and 2013 respectively. He received his master's degree in computer engineering from Missouri University of Science and Technology in May 2015.